Localization in the one-dimensional quantum chain with nonreciprocal disorder

Jia-Rui Li,[1] Shu-Feng Zhang,[2,*] Lian-Lian Zhang,[1] and Wei-Jiang Gong[1,†]
[1]*College of Sciences, Northeastern University, Shenyang 110819, China*
[2]*School of Physics and Technology, University of Jinan, Jinan 250022, China*

(Received 6 February 2024; revised 27 May 2024; accepted 25 July 2024; published 6 August 2024)

We propose the one-dimensional structure driven by nonreciprocal disorder in the coupling terms of a quantum chain, probing the properties of localization and the skin effect of the system under the competition between disorder and nonreciprocal coupling. The results indicate that such disorder has a significant modulating effect on the energy spectra and localization of the system. To be specific, it induces the pseudo-Hermitian symmetry phase transition in the system. And when the disorder parameters in the two hopping directions are the same, some states have opportunities to localize on the left and right sides. The interesting result is that a localization transition appears at weak disorder strength, and its occurrence is related to the energies of states. Next, when the disorder parameters in the two hopping directions differ, the energy-dependent non-Hermitian skin effect is induced, accompanied by the more intricate localization phenomena. We believe that the findings in this work will enhance the understanding of nonreciprocal disorder effects on one-dimensional quantum systems.

DOI: 10.1103/PhysRevB.110.085409

I. INTRODUCTION

The concept of Anderson localization, first proposed in disordered solid materials in 1958, suggested that electronic states could be localized within a certain energy range [1]. The introduction of the theory of Anderson localization led to widespread discussions on the subject. The development of the scalar theory by Abrahams *et al.* in 1979 further deepened our understanding of localization and the metal-insulator transition in electronic systems [2]. It has been found that in one- and two-dimensional systems, electronic states are always localized as long as there is disorder present. In contrast, for three-dimensional systems, localized and extended states can coexist in different energy ranges separated by mobility edges [2]. Advances in quantum mechanics and condensed-matter physics led to the fabrication of new materials and systems for which localization phenomena induced by disorder have become the hot topic of research. Anderson localization has also been extended to the fields of condensed matter, light, and cold atoms [3–7]. In addition, inspired by Anderson localization driven by random disorder, the localization transition in various quasiperiodic systems has also been reported from different aspects [8–11].

With the extension of the concept of topology to physics, topological materials have become attractive. Efforts have been made to explore topological phases in various topological materials with the aim of finding various edge states for future nanoelectronics and quantum computing. Researchers have also combined topological materials with the fundamentals of Anderson localization, and their in-depth studies have given it new meaning [12–15]. According to numerous articles on the study of topological properties [16–20], we can characterize the existence of a system's edge states by using topological invariants. Such topologically protected edge states are robust to certain types and degrees of disorder [16–18]. Because the introduction of disorder could destroy the periodic boundary condition of the system, it has been assumed that the presence of disorder tends to suppress topological properties. However, it has been found that in topological insulators, disorder can induce a phase transition from topologically trivial to nontrivial regions [15,21–23]. Subsequently, some groups have demonstrated that disorder leads to topological phase transitions even in other topological materials [24,25]. This means that in topological systems, disorder plays a special role in modulating the phase transitions in addition to the conventional localization phenomena. Also, the interplay between topology and disorder can pave the way for new areas of research in topological materials.

On the other hand, non-Hermitian systems have been attracting a great deal of interest from both theoretical and experimental physicists [26–31]. There are currently two main realizations of non-Hermitian mechanisms. The first is the gain-loss potentials [32–36]. The best known gain-loss non-Hermitian systems are parity-time ($\mathcal{PT}$) symmetric systems with gain and loss imaginary potentials. As suggested by Bender and Boettcher in 1998, such systems have the potential to show a completely real energy spectrum [37,38]. Subsequently, the $\mathcal{PT}$ symmetric imaginary potential was combined with topological systems to study the mechanisms of new topological phase transitions and $\mathcal{PT}$-symmetry shifts appearing in the systems, such as the one-dimensional Su-Schrieffer-Heeger (SSH) model, the trimer lattice, the two-dimensional SSH lattice, the Kitaev model, and graphene [39–47]. In the experiments, $\mathcal{PT}$-symmetric systems can be achieved in topological circuits [48–50], photonic structures [51–53], and optics [54–56]. The other non-Hermitian

*Contact author: sps-zhangsf@ujn.edu.cn
†Contact author: gwj@mail.neu.edu.cn

mechanism is the nonreciprocal coupling caused by the asymmetric strength of the hopping amplitudes between the lattice points, which causes the systems to display the non-Hermitian skin effect (NHSE) [57–61]. Due to the occurrence of the NHSE, the bulk-boundary correspondence of the system completely collapses [57,62]. Accordingly, the topological characteristics in nonreciprocal topological structures have been discussed with the help of concepts such as the generalized Brillouin zone (GBZ) [57,63–65], non-Bloch bulk-boundary correspondence [57], and non-Bloch topological invariants [57,63].

The theoretical and experimental development of non-Hermitian systems has encouraged researchers to focus on the effect of disorder on those systems [66–68]. The most famous work is the Hatano-Nelson model [69–71], in which the asymmetric hopping terms induced by imaginary normative fields lead to the existence of the localization-delocalization transition and the mobility edge [72]. Since then, more interesting results have been reported by different groups. For instance, in non-Hermitian Weyl semimetals, disorder could induce the appearance of a flat band [73]. Stefano proposed the Hatano-Nelson model with unidirectional hopping under on-site potential uncorrelated disorder on the complex energy plane, and predicted rather generally three distinct spectral phases for the energy spectra under both open and periodic boundary conditions [74]. In the dimerized Kitaev superconductor chain, the non-Hermitian disorder-driven topological transition has been observed, offering a new opportunity for the realization of a Majorana zero mode [67]. The disorders have been found to drive the phase transition in the second-order non-Hermitian skin effect [76]. In disordered systems with a single non-Hermitian impurity, anomalous skin effects have been demonstrated [77]. In addition, researchers considered one-dimensional nonreciprocal systems with random variations over a continuous time step, and such systems have been found to display the stochastic skin effect [78].

Based on existing works, one can find that disorder indeed brings about the nontrivial effect in non-Hermitian systems by inducing new phase transitions. Meanwhile, the types of disorder can also determine the variation in the properties of non-Hermitian systems. In the present work, we would like to investigate the localization phenomena in a one-dimensional (1D) quantum chain. These phenomena are driven by one new type of disorder, i.e., nonreciprocal disorder. The calculation results show that such disorder plays a special role in creating the band structure by inducing the pseudo-Hermitian symmetry phase transition. In addition, such disorder can adjust the localization of states. Moreover, this type of disorder does not localize all eigenstates immediately, and the localization transition occurs under weak disorder. When the disorder parameters are adjusted to differ from each other, this system displays the energy-dependent NHSE and localization of states, as well as the transition from unidirectional to bidirectional localization. These results can help us to understand the effects of nonreciprocal disorder on 1D quantum systems.

The specific content of this paper is organized as follows: In Sec. II, we introduce the Hamiltonian and analyze the symmetry of the system. We also display the expressions of the disorder-averaged inverse participation ratio (IPR) and the localization length. In Sec. III, we discuss in detail the energy spectra and localization properties of the two disorder configurations H_1 and H_2 as the disorder strength varies, and for different random number regimes in terms of the energy bands, the disorder-averaged probability densities, and the localization lengths. Section IV provides a summary. Finally, in the Appendixes, we provide the condition of pseudo-Hermitian symmetry by using hopping terms and calculating the real eigenenergy level statistics.

II. MODEL AND THEORY

This work concentrates on a 1D quantum chain affected by nonreciprocal disorder. In this system, a spinless particle hops along a 1D chain with finite disorder added to the hopping terms. The corresponding Hamiltonian is written as

$$H = \sum_j (t_{1,j} c_j^\dagger c_{j+1} + t_{2,j} c_{j+1}^\dagger c_j). \tag{1}$$

$c_j^\dagger$ (c_j) denotes the creation (annihilation) operator on the site j. The total system has L sites. $t_{1,j}$ and $t_{2,j}$ are the hopping terms from right to left and from left to right, respectively. According to the imposition of disorder terms in the Anderson disorder system, we define $t_{1,j} = t + \frac{d}{2} W_{1,j}$ and $t_{2,j} = t - \frac{d}{2} W_{2,j}$, where d describes the strength of disorder, and $W_{1(2),j}$ is the number drawn at random from a uniform distribution. Surely, due to the presence of disorder, the random hopping strengths cause the hopping terms to be spatially uncorrelated with $t_{1,j} \neq t_{2,j}$. The nonreciprocity property comes up when there is a difference in hopping between neighboring lattices, and non-Hermitian mechanisms are introduced in the system.

According to Eq. (1), we are allowed to express the real-space Hamiltonian in its matrix form based on $\Psi = (\psi_1, \psi_2, \psi_3, \ldots, \psi_{L-1}, \psi_L)^T$, i.e.,

$$H = \begin{bmatrix} 0 & t_{1,1} & 0 & \cdots & 0 \\ t_{2,1} & 0 & t_{1,2} & \cdots & 0 \\ 0 & t_{2,2} & 0 & \ddots & \vdots \\ \vdots & \ddots & \ddots & \ddots & t_{1,L-1} \\ 0 & \cdots & 0 & t_{2,L-1} & 0 \end{bmatrix}. \tag{2}$$

With the help of such a matrix form, we can judge the symmetry of this system. First, it can be found that this system has the chiral symmetry $\Gamma H \Gamma^{-1} = -H$, with $\Gamma = \mathrm{diag}(1, -1, 1, -1, \ldots)_{L\times L}$. Moreover, it also has the pseudo-Hermitian symmetry (PHS) $\eta H \eta^{-1} = H^\dagger$, where

$$\eta = \mathrm{diag}\left\{1, \frac{t_{1,1}}{t_{2,1}}, \frac{t_{1,1}t_{1,2}}{t_{2,1}t_{2,2}}, \ldots, \frac{t_{1,1}t_{1,2}\cdots t_{1,L-1}}{t_{2,1}t_{2,2}\cdots t_{2,L-1}}\right\}.$$

The existence of PHS signifies that the system could display purely real energy [79,80]. In the presence of the imaginary part of the energy, the system will undergo the PHS phase transition. If all states have their real energies, the system will be located in the protected PHS phase. Otherwise, the broken PHS phase comes into being with the finite imaginary part of the energy.

To present a comprehensive description of the skin effect, localization, and other features of our considered system, we would like to carry out discussions by introducing some physical observables, such as the inverse participation ratio, and localization lengths.

A. Disorder-averaged IPR and directional IPR

To begin with, we introduce the disorder-averaged inverse participation rate (dIPR) [67,75] to characterize the effect of disorder and to analyze the skin effect and localization of the wave function. The specific expression of dIPR is written as

$$\mathrm{dIPR_n} = \frac{1}{M}\sum_{m=1}^{M}\mathrm{IPR_n} = \frac{1}{M}\sum_{m=1}^{M}\frac{\sum_j |\psi_{n,j}|^4}{\left(\sum_j |\psi_{n,j}|^2\right)^2}. \tag{3}$$

Here $\mathrm{IPR_n}$ is the inverse participation ratio, $\psi_{n,j}$ is the right eigenstate component of ψ_n at site-j under the nth eigenstate, and ψ_n satisfies the Schrödinger equation $H\psi_n = E_n\psi_n$, with H being the model Hamiltonian and E_n the nth eigenenergy. In this expression, M is the number of disordered configurations. According to Refs. [67,82,83], we know that for the extended states, $\mathrm{IPR_n}(\mathrm{dIPR_n}) \sim 1/L$ and it tends to be equal to zero in the case of $L \to \infty$. Alternatively for the localized states, these two quantities will manifest as nonzero finite values.

According to Refs. [31,81,84], on the basis of the IPR, we use the directional IPR(χ) to characterize the localization of all eigenstates. The specific definition equation can be written as

$$\chi_n = \mathrm{sgn}\left[\sum_j^L \left(j - \frac{L}{2} - \beta\right)|\psi_{n,j}|\right]\frac{\sum_j |\psi_{n,j}|^4}{\left(\sum_j |\psi_{n,j}|^2\right)^2}. \tag{4}$$

Here, the definition of $\psi_{n,j}$ is consistent with that in the dIPR, and β is a constant usually determined as $0 < \beta < 0.5$. In this work, we perform disordered averaging and set $\beta = 0.2$. $\mathrm{sgn}(x)$ represents the sign function, in which $\mathrm{sgn}(x) = -1.0$ when $x < 0$ but $\mathrm{sgn}(x) = 1.0$ if $x > 0$. By observing the value of χ_n to be positive or negative, one can determine whether the wave function of eigenstate-n has a tendency to be of right or left localization.

B. Localization length ξ

To describe the localization phenomenon, we should calculate the localization length ξ to determine the localization effect of our considered system [66,85]. According to the Schrödinger equation $H\Psi = E\Psi$, we can obtain the relationship

$$t_{2,j-1}\psi_{j-1} + t_{1,j+1}\psi_{j+1} = E\psi_j. \tag{5}$$

Such a series of equations allows us to write out the following expression:

$$\begin{bmatrix}\psi_{j-1}\\ \psi_j\end{bmatrix} = M_{\mathcal{L},j}\begin{bmatrix}\psi_j\\ \psi_{j+1}\end{bmatrix}, \quad \begin{bmatrix}\psi_{j+1}\\ \psi_j\end{bmatrix} = M_{\mathcal{R},j}\begin{bmatrix}\psi_j\\ \psi_{j-1}\end{bmatrix}. \tag{6}$$

Based on the result in Eq. (5), we can obtain the concrete form of the transfer matrix $M_{\mathcal{L},j}$ and $M_{\mathcal{R},j}$:

$$M_{\mathcal{L},n} = \begin{bmatrix} t_{2,j-1}^{-1}E & -t_{2,j-1}^{-1}t_{1,j+1}\\ 1 & 0\end{bmatrix}, \tag{7}$$

$$M_{\mathcal{R},n} = \begin{bmatrix} t_{1,j+1}^{-1}E & -t_{1,j+1}^{-1}t_{2,j-1}\\ 1 & 0\end{bmatrix}. \tag{8}$$

Thus, we can solve the localization length $\xi_{L(R)}$ of the left (right) direction by calculating the inverse of the smallest positive eigenvalue of the 2×2 matrix [70,86], i.e., $(\prod_{j-1}^{L} M_{\mathcal{L}(\mathcal{R}),j})(\prod_{j-1}^{L} M_{\mathcal{L}(\mathcal{R}),j})^{\dagger}$.

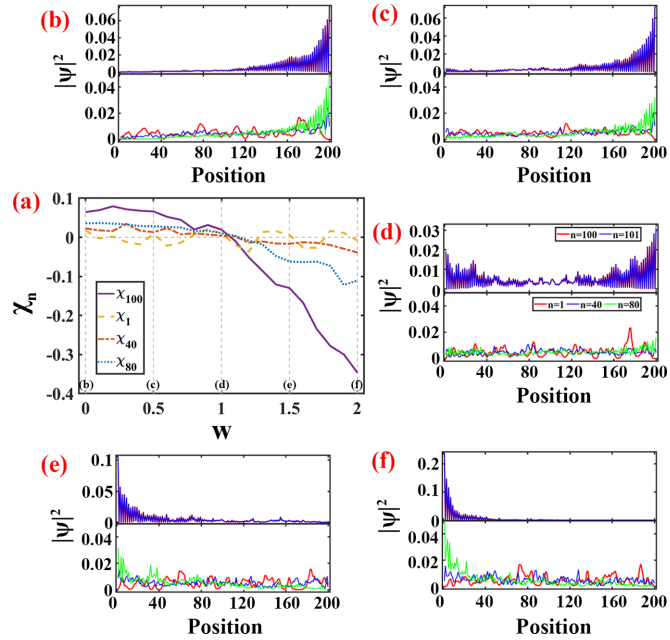

FIG. 1. (a) The spectra of χ_n with the increase of w at $d = 1.0$. The purple, yellow, red, and blue lines indicate the energy level index at $n = 100$, 1, 40, and 80, respectively. (b)–(f) Disorder-averaged probability density distributions of the corresponding energy level for the cases of $w = 0$, 0.5, 1.0, 1.5, and 2.0. In detail, $n = 1$ is the absolute energy maximum $|E|_{\max}$, $n = 100$ (101) is the absolute energy minimum $|E|_{\min}$, and $n = 40$ (80) is the eigenstate between $|E|_{\max}$ and $|E|_{\min}$.

III. RESULTS AND DISCUSSIONS

Following the theory presented in the preceding section, we perform numerical calculations to investigate the energy band structure of our system under an open boundary condition in order to observe the localized properties in detail. To present a comprehensive analysis, we take the disorder strength $d > 0$, and the two kinds of disorder random numbers are set as $W_{1,n} \in [-1.0, 1.0]$ and $W_{2,n} \in [-w, w]$ with $w \in [0, 2.0]$.

First, we focus on the effect of the variation of random numbers in terms of disorder. Figure 1 displays the spectra of χ_n with w increasing from 0 to 2.0. The purple, yellow, red, and blue lines in Fig. 1(a) describe the energy level index at $n = 100$, 1, 40, and 80, respectively. From Fig. 1(a), we find that $\chi_{n=40,80,100}$ are always greater than zero in the case of $0 < w < 1.0$. Thus, the system tends to be localized on the right side of the system. With the increase of w, the value of χ_n decreases and becomes smaller than zero in the range of $w > 1.0$. This suggests that the eigenstates of this system undergo a right-to-left localization transition. In Figs. 1(b)–1(f), we present the disorder-averaged probability density distributions of the corresponding energy levels for $w = 0$, 0.5, 1.0, 1.5, and 2.0, respectively. We can observe a similar phenomenon to Fig. 1(a). In the range of $0 < w < 1.0$, the eigenstates of $\chi_{n=40,80,100}$ are localized on the right side [as shown in Figs. 1(b) and 1(c)]. When $w = 1.0$, as shown

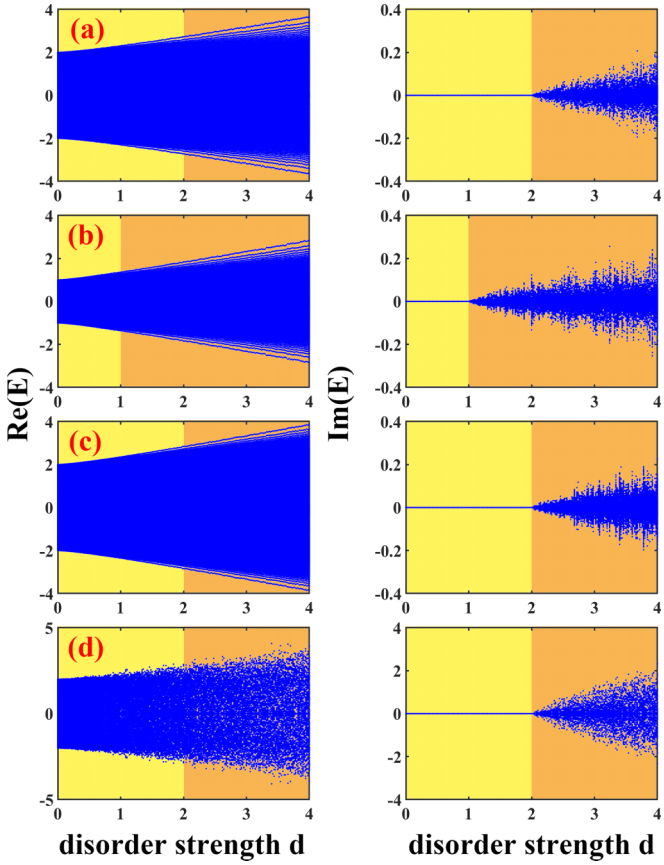

FIG. 2. (a)–(c) Real and imaginary energy spectra of (a) $(t, L) = (1.0, 200)$, (b) $(t, L) = (0.5, 200)$, and (c) $(t, L) = (1.0, 500)$. The spectra are the average over 100 disorder configurations. (d) The specific real and imaginary energy spectra in the case of $(t, L) = (1.0, 200)$ for only one disorder configuration. The yellow and orange colors in these four cases identify the regions of protected and broken PHS phases, respectively.

in Fig. 1(d), the eigenstates are localized at both ends. In the range of $w \in [1.0, 2.0]$ [see Figs. 1(e) and 1(f)], it can be observed that the corresponding eigenstates exhibit a clear localization effect towards the left side of the system. Accordingly, the change of parameters has a significant effect on the localization properties.

Based on the above results, we next discuss the energy spectra and localization properties in two different disordered configurations, i.e., (I) $H_1 \rightarrow \{W_{1,n} \in [-1.0, 1.0], W_{2,n} \in [-1.0, 1.0]\}$; (II) $H_2 \rightarrow \{W_{1,n} \in [-1.0, 1.0], W_{2,n} \in [-0.5, 0.5]\}$.

A. Configuration of H_1

We start by discussing the first configuration, which is described as $H_1 \rightarrow \{W_{1,n} \in [-1.0, 1.0], W_{2,n} \in [-1.0, 1.0]\}$. First, we would like to consider the short chain and concentrate on the band-structure properties by observing the energy spectra and wave function. Based on previous work [87], the disorder-averaged eigenenergies are given as $E_n = \frac{1}{M}\sum_{m=1}^{M} E_n^{(m)}$.

Figure 2 shows the real and imaginary energy spectra in different cases, where the left column denotes the real part and the right is the imaginary part of the energy. From the energy spectra, we can clearly find the appearance of $\mathrm{Im}(E)$, and its range becomes wide with an increase of disorder strength d. This means that in this system, the PHS phase transition occurs, leading to the presence of two different phase regions, i.e., the protected PHS phase (yellow region) and the broken PHS phase (orange region). Specifically, in the case of $t = 1.0$ and $L = 200$ [see Fig. 2(a)], the system undergoes the PHS phase transition at $d = 2.0$. When disorder strength is taken to be $0 < d < 2.0$, the eigenenergies are real, since the system is protected by PHS. In the case of $d > 2.0$, the imaginary eigenenergies are not equal to zero anymore with the occurrence of PHS breaking. When $t = 0.5$ [see Fig. 2(b)], the region of $0 < d < 1.0$ is manifested as the protected PHS phase in which the eigenenergies are real. In the region of $d > 1.0$, the eigenenergies contribute their imaginary part and then the system enters the broken PHS phase. Thus, we can think that the real energy spectra are generated by the pseudo-Hermitian symmetry. In addition, we increase the chain length, such as $L = 500$ at $t = 1.0$ in Fig. 2(c). It can be found that the system still undergoes the PHS phase transition at $d = 2.0$, and the region of the imaginary part $\mathrm{Im}(E) \neq 0$ is widened. These results are the same as those presented in Fig. 2(a). The above-mentioned phenomena not only occur in the energy bands under disorder averaging, but they also hold for one disordered configuration. For example, Fig. 2(d) shows the specific real and imaginary energy spectra in the case of $(t, L) = (1, 200)$ for only one disorder configuration. We can find that the PHS phase transition occurs at $d = 2.0$, which is the same as the results shown in Fig. 2(a). Therefore, we infer that there is a numerical relationship between the change in t and the PHS phase-transition conditions. Moreover, the increase in the chain length does not change the critical phase-transition conditions for the two phases.

To further understand the phenomenon of PHS phase transitions in our system, we discuss the effects of t, d, and L in Fig. 3. Here we introduce the imaginary-energy ratio [83], which can assist in demonstrating the appearance of complex energy eigenstates. The corresponding expression is given as

$$\rho = \frac{1}{L}\sum_{n=1}^{L} \varepsilon(|\mathrm{Im}(E_n)|). \tag{9}$$

In this expression, $\varepsilon(x)$ is the step function. When $\rho = 0\,(1.0)$, all the eigenenergies are purely real (imaginary). In the region of $0 < \rho < 1.0$, the system belongs to the mixed phase with real and imaginary energies.

Figure 3(a) displays the phase diagram for the imaginary-energy ratio as a function of t and d at $L = 200$, with the color corresponding to the value of ρ. Here, we can observe that when the parameters are located in the range of $t > d/2$, ρ is equal to zero. This means that all the eigenenergies are real, and the system is in the protected PHS phase region. Alternatively for $0 < t < d/2$, $\rho > 0$. In such a case, the system is characterized as the broken PHS phase. For example, in the cases of $t = 0.5$, 1.0, and 1.5, as shown in Fig. 3(b), the conditions for the PHS phase transition in the three cases are $d = 1.0$, 2.0, and 3.0, respectively. Such results are consistent with the spectra in Figs. 2(a) and 2(b).

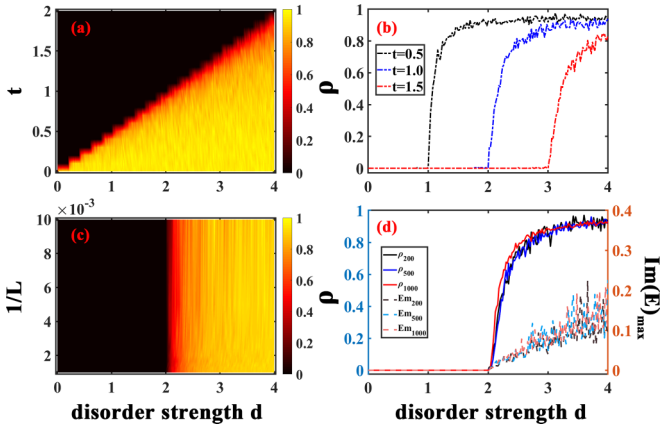

FIG. 3. (a) Phase diagram for the imaginary-energy ratio ρ as a function of t and d at $L = 200$. (b) The specific results of $t = 0.5$ (black line), $t = 1.0$ (blue line), and $t = 1.5$ (red line) at $L = 200$. (c) The phase diagram for IER as a function of d and L at $t = 1.0$. (d) $L = 200$ [black (light-black) line], $L = 500$ [blue (light-blue) line], and $L = 1000$ [red (light-red) line] represent the IER (maximum value of the imaginary energy), respectively.

Therefore, we can conclude that the condition for the system to undergo the PHS phase transition is exactly expressed as $d = 2t$. We can also explain this condition by the hopping terms (as shown in Appendix A). In addition, Figs. 3(c) and 3(d) show the relationship among ρ, $1/L$, and d. According to the phenomenon in Fig. 3(c), we infer that the length of the system does not affect the condition of the PHS phase transition, and the phase-transition condition is maintained as $d = 2t$ with an increase of length L. Figure 3(d) shows that the conditions of the three cases are the same as $d = 2.0$ (see the solid lines). In addition, we introduce the maximum value of the imaginary part of the energy at $L = 200$, 500, and 1000, respectively. The maximum value of the imaginary part $\mathrm{Im}(E)_{\max}$ also appears in the region of $d > 2.0$ (see the dashed lines). Therefore, we can conclude that the chain length does not change the condition of the PHS phase transition.

Figure 4 displays the dIPR to illustrate the wave-function localization effect of H_1 under a short chain with $L = 200$. The x-axis represents the strength of the disorder d, and the y-axis represents the energy index, where $n = 1$ and 200 means the energy band edges $-E_{\max}$ and $E_{\max}$, respectively, and $n = 100$ means the absolute minimum of the energy $|E|_{\min}$. The color denotes the value of the dIPR, and the change in

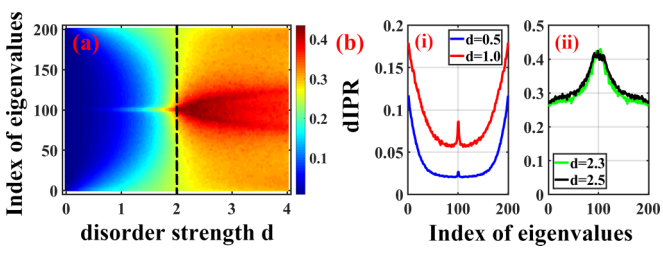

FIG. 4. (a) The disorder-averaged inverse participation rate (dIPR) with the change of d and index of eigenvalues, respectively. (b) The specific results of $d = 0.5$ (blue line) and $d = 1.0$ (red line) of the protected PHS phase in the left column (i), and the results of $d = 2.3$ and 2.5 of the broken PHS phase in the right column (ii).

color to red corresponds to the increase of the dIPR value and the strengthening of the localization effect in this process. Figure 2(a) shows that the system comprises two kinds of phases, namely the protected PHS phase ($0 < d < 2$) and the broken PHS phase ($d > 2$). We can find that they exhibit different results of dIPR for the protected and broken PHS phases. Specifically, in the protected PHS phase, when $d = 0$, dIPR $\to 0$, indicating weak localization. In the case of small d, the dIPR values for the higher-energy states are higher than those for the lower-energy states. In particular, near the edges of the energy band, higher dIPR values can be observed. For example, in the case of $d = 0.5$ and 1.0 [as shown in Fig. 4(b)(i)], the value of dIPR in $n = 1$ and 200 is larger than the value of $n = 100$. Thus, the states near the edges of the band are more prone to be localized than states near the band center. With the increase of disorder strength, dIPR of the states near $E = 0$ is gradually enhanced, such as the case of $d = 1.0$ [see Fig. 4(b)(i)]. In the broken PHS phase, the dIPR of lower-energy states is larger than that of higher-energy states, such as the cases of $d = 2.3$ and 2.5 in Fig. 4(b)(ii). Based on these results, it can be seen that the protected and broken PHS phases will show different localization effects, and the energy magnitude has its special influence on the localization effect of H_1.

According to Fig. 1(c), when $w = 1.0$, the eigenstates could be localized at both ends. Thus, in this part, we discuss the wave-function probability density distribution in detail with the change of disorder strength d. Figure 5 plots the disorder-averaged probability density spectra to show the localization phenomena of our system. In the case of $d = 0.5$, the lower-energy states tend to be localized at both ends of the system, especially the states of $n = 100$ (101). This trend becomes less pronounced as the absolute value of energy increases, especially the states of $n = 40$ (80). For the higher-energy states (such as $n = 1$), the disorder-averaged probability density reaches its extremum at the middle of the chain. With the increase of d, the trend of localization at both ends of the system becomes more pronounced. Taking the case of $d = 1.5$ as an example, one can see in Fig. 5(b) that states of $n = 100$ (101) present better localization than the case of $d = 0.5$. When d increases to 2.5, the system begins to obtain the imaginary part of the energy. From Fig. 5(c), it is found that the effects of localization at the left and right sides present themselves in the states with near zero energy, e.g., $n = 107$. In addition, the localization effect for $n = 100$ (101) is not manifest with this trend. For higher-energy states, the localization effect of the system becomes more apparent.

To investigate why the disorder-averaged probability density appears to be localized at the two ends, we plot the wave function under partial disorder configurations, as shown in the rightmost column of Figs. 5(a)–5(c)(ii). It is shown that the localization effects at both ends of the system consist of the superposition of eigenstates averaged over different disordered configurations, including eigenstates localized on the left or right sides (blue or red line) and a small number of eigenstates localized at the middle of the chain. For $n = 1$, the disorder-averaged eigenstates comprise the superposition of highly localized eigenstates. These probability density distribution results for the wave functions are quite different

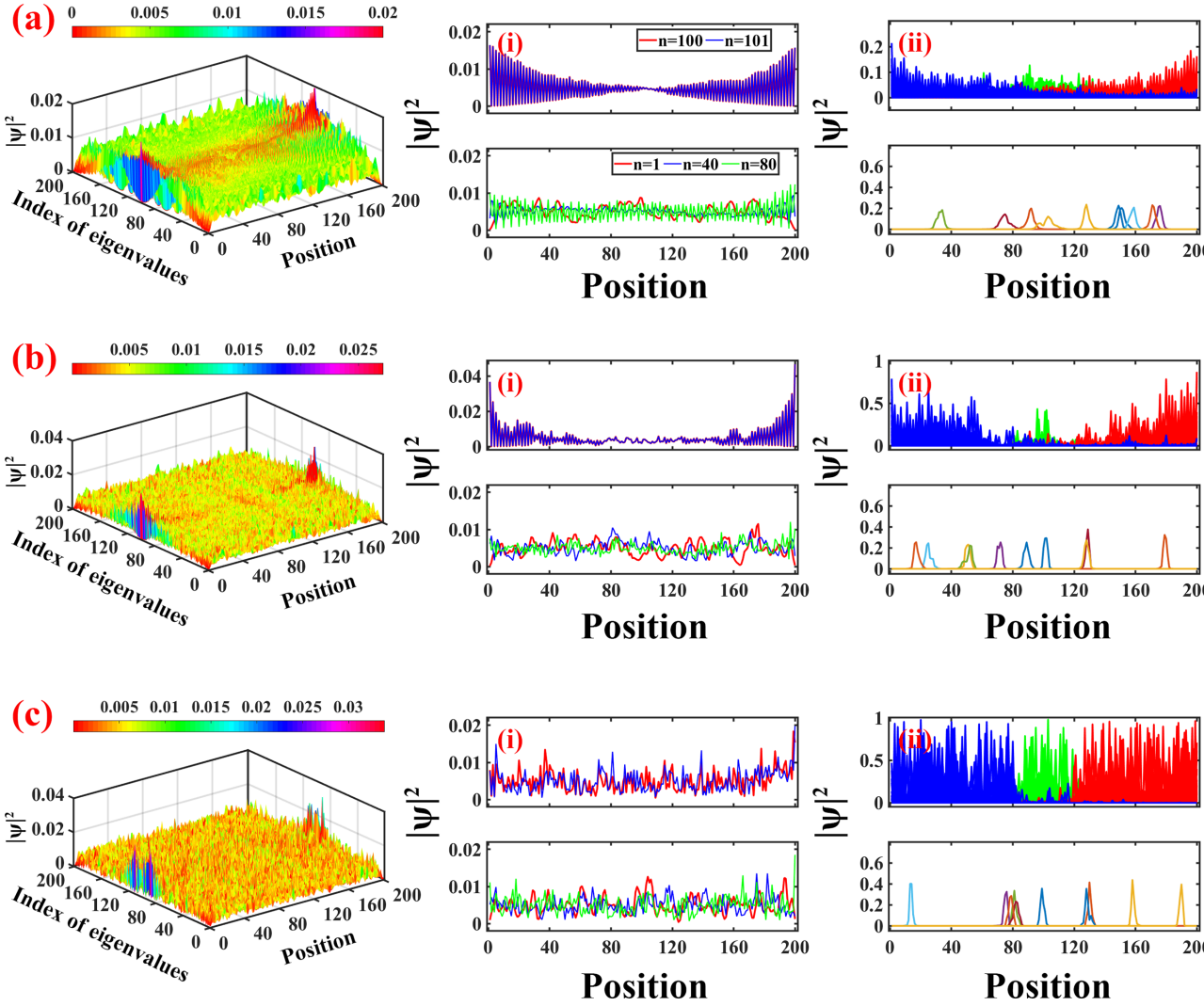

FIG. 5. (a)–(c) (i) The disorder-averaged probability density spectra of $d = 0.5,\ 1.5$, and 2.5, respectively. (ii) The right column shows the specific results in part of different disorder configurations. In addition, $n = 1$ is the absolute energy maximum $|E|_{\max}$, $n = 100$ (101) is the absolute energy minimum $|E|_{\min}$, and $n = 40$ (80) is the eigenstate between $|E|_{\max}$ and $|E|_{\min}$. The total unit cell L is equal to 200.

from the effect of the NHSE that produces all eigenstates localized on one side of the system after the introduction of conventional nonreciprocal coupling [57].

Next, we focus on the long chain $L = 10\,000$. With a view to better observing the localization effects of the two regions driven by disorder, we calculate the left and right localization lengths ξ_L and ξ_R. Figures 6(a) and 6(b) show the variation of the left (right) localization length ξ_L (ξ_R) with the disorder strength and eigenenergies when the chain length $L = 10\,000$. As is known, for the conventional 1D Anderson model, disorder leads to direct localization of the eigenstates [1,88,89]. However, in Fig. 6 it can be seen from the localization phase diagram that the disorder does not localize all eigenstates immediately, and the eigenstates close to zero energy still show the process of localization transition. This is completely different from the traditional 1D Anderson model. In addition, this localization transition only occurs in the protected PHS phase. Specifically, Figs. 6(c)–6(e) show the results at $E = 0.05,\ 1.0$, and 2.0 in the protected PHS phase, respectively. The lower-energy states and near-zero-energy states need larger disorder strength to undergo the localization phase transition compared to the higher-energy states. For example, in the cases of $E = 0.05$ in Fig. 6(c), the localization length $\xi_L = \xi_R \gg L$ when $d = 0$, so the system appears as the extended states. When $d > 0.2$, $\xi_L, \xi_R < L$, the system begins to exhibit the localization trend. With the increase of d, the system undergoes the localization transition. For the case of $E = 1.0$, the system displays similar phenomena with $E = 0.05$. Next, for higher-energy states with $E = 2.0$, the system has a weak localization effect at $d = 0$. This indicates that the eigenstates close to the band edges are more prone to localization than those close to the band center. It can also be observed that both the left and right localization lengths gradually converge to zero with an increase of disorder, which indicates that the system undergoes localization in two directions. For the result of the broken PHS phase, ξ_L and ξ_R both satisfy $\xi_{L(R)} < L$, and the left and right directions are both manifest as the localization effect, in agreement with the results in Fig. 6(f). We can also observe the localization transition using level statistics (Appendix B).

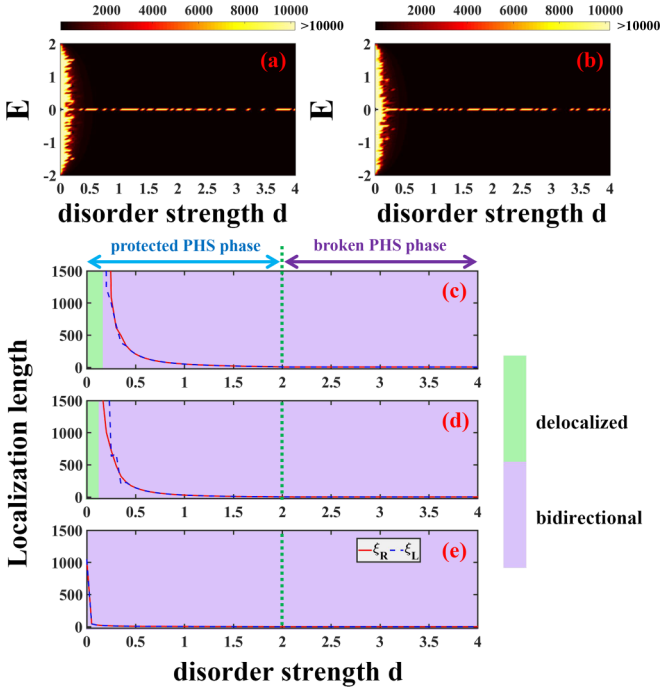

FIG. 6. (a),(b) Spectra of the left and right localization lengths ξ_L and ξ_R of eigenenergy-disorder $(E - d)$, respectively. (c)–(e) Left and right localization lengths for $L = 10\,000$ in the protected and broken PHS phases at energy $E = 0.05$, 1.0, and 2.0, respectively. The dotted blue line describes ξ_L, and the solid red line indicates ξ_L. In (c)–(e), the green region means the delocalized states, and purple regions indicate the states that satisfy bidirectional localization.

Following the above discussion, we would like to summarize the effects of disorder on the band structure and localization of H_1: For the band structures, (I) the increase of disorder strength d can drive the PHS phase transition at $d = 2t$. The disorder leads to the existence of two different phase regions of the system: one is the protected PHS phase with real-energy eigenstates, and the other is the broken PHS phase with nonzero $\mathrm{Im}(E)$. (II) The length of the chain cannot change the condition of the PHS phase transition.

As for the wave function, nonreciprocal disorder does not induce the traditional NHSE, but rather a new localization phenomenon of energy-modulated localization on both sides of the system. (I) In the protected PHS phase, the lower-energy states, especially near-zero-energy states, tend to be localized at the left and right sides of the system. Under the same disorder condition, the trend of localization on the left and right sides is weakened with the increase of energy. In addition, the high-energy states show a tendency to be localized by the superposition of highly localized eigenstates. (II) In the broken PHS phase, the localization effect is stronger for the lower-energy states than the higher-energy states. Although the tendency of localization at the ends of the system still exists for the lower-energy states, it does not correspond to the absolute minimum of energy.

Next, for the localization result, the disorder does not immediately localize all eigenstates. The disorder leads to a localization transition that is different from that of the 1D Anderson model. (I) The localization transition only occurs

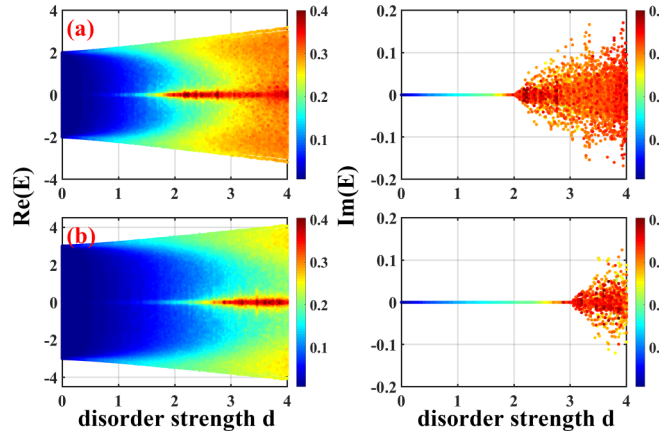

FIG. 7. (a),(b) Real and imaginary energy spectra of (a) $(t, L) = (1.0, 200)$ and (b) $(t, L) = (1.5, 200)$. The color indicates the value of dIPR.

in the region of protected PHS phase with weak disorder. (II) When the disorder strength is greater than the critical strength, all eigenstates, both higher- and lower-energy states, become localized and exhibit bidirectional (left and right) localization effects in protected and broken PHS phases.

B. Configuration of H_2

The above discussion shows that the nonreciprocal disorder not only changes the band-structure properties, but it also regulates the localization effects at different energies. In view of this fact, we would like to investigate the second disorder configuration, in which $H_2 \to \{W_{1,n} \in [-1.0, 1.0], W_{2,n} \in [-0.5, 0.5]\}$. Our purpose is to clarify the occurrence of the NHSE.

For the configuration of H_2, we also start by focusing on the properties of the band structure in a short chain, $L = 200$. Figures 7(a) and 7(b) show the real and imaginary energy spectra of $t = 1.0$ and 1.5 with $L = 200$. First, it can be found that the conditions for the PHS phase transition also obey the relationship $d = 2t$. The region of the imaginary part of the energy becomes steadily wider with the increase of d. This means that the system also has two types of phase regions, i.e., the protected PHS and broken PHS phases. These results are similar to the band structure of the configuration of H_1. Similarly, we explain the PHS phase-transition condition for H_2 by hopping terms in Appendix A. From the value of dIPR, we can get similar results with H_1. In the broken PHS phase, when d is small, the higher-energy states near the edges of the energy band have greater dIPR values than the lower-energy states near zero energy. With the increase of d, the value of dIPR increases near the zero-energy position. In the broken PHS phase, the localization effect of states near $E = 0$ is stronger than that of other states. Therefore, the energy band results indicate that the configuration of H_2 also undergoes the PHS phase transition, and the two phases also have different properties.

From Fig. 1(c), we know that the eigenstates could be localized on the right side. To better understand this process, Figs. 8(a)–8(d) show the disorder-averaged probability density spectra for $d = 0.1$, 1, 1.5, and 2.5 in $L = 200$,

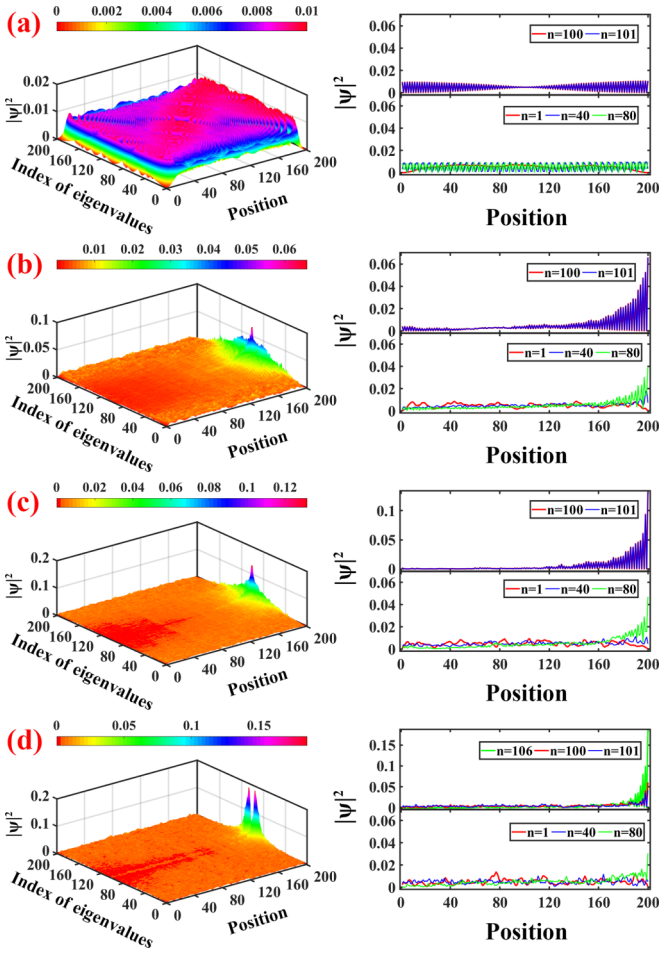

FIG. 8. (a)–(d) The disorder-averaged probability density spectra of $d = 0.1,\ 1.0,\ 1.5$, and 2.5, respectively. The right column shows the specific results in each case.

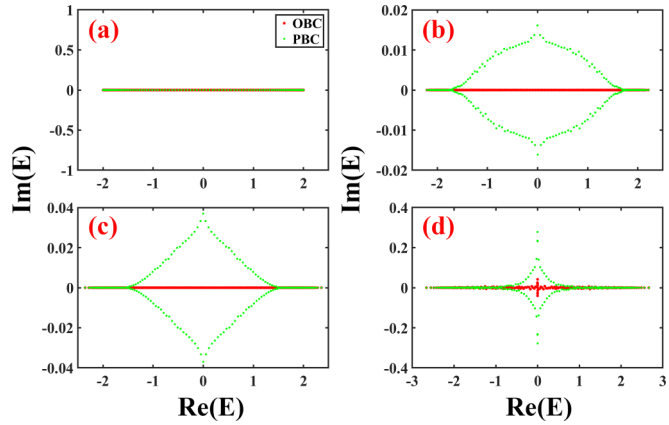

FIG. 9. (a)–(d) The disorder-averaged energy spectra under PBC and OBC for $d = 0$, 1.0, 1.5, and 2.5, respectively. The red line indicates the OBC case, and the green line indicates the PBC case.

respectively. In the case of $d = 0.1$, as shown in Fig. 8(a), most states are not localized at the boundary. Thus the states are mainly extended, such as the results in the right column. With the increase of d, e.g., $d = 1.0$ in Fig. 8(b), we can clearly observe that in the region where the energy level index ranges from $n = 40$ to 80, the wave function tends to be localized on the right side of the system. And then the NHSE comes up in the lower-energy region. As the energy approaches zero, this skin effect becomes more pronounced, such as $n = 100$ (101). Such a result is completely different from H_1. The higher-energy states at and near the band edges exhibit the localization effect distributed throughout the system, as shown in the case of $n = 1$. This effect also leads to a superposition average of disordered configurations, similar to H_1. Although the system displays the skin effect, it is not satisfied by all states. Thus, this is different from the traditional NHSE, so we define it as the energy-dependent NHSE. When the disorder strength increases to 1.5, the region of the energy-dependent NHSE is reduced compared to the case of $d = 1$. This indicates that the disorder-averaged probability density of partial eigenstates no longer shows a tendency to be localized on the right side, such as the eigenstate with $n = 40$. In contrast, eigenstates near zero energy still retain the energy-dependent NHSE, such as the state for $n = 80$. The energy-dependent NHSE is more pronounced when the eigenstate energies are close to zero energy [see the states for $n = 100$ (101)]. At this point, the wave-function density at the left end is close to zero, manifested as red in the wave-function phase diagram. The localization of higher-energy states is similar to the case of $d = 1$. In the broken PHS phase, the region with NHSE is significantly reduced, and the peak is no longer at $n = 100$ (101), rather it is at $n = 107$ (94).

From the disorder-averaged wave-function probability density, it is easy to see that the system exhibits a phenomenon not present in the H_1 configuration, namely the energy-dependent non-Hermitian skin effect. According to the previous work [74], we can explain this phenomenon by analyzing the relationship between the periodic boundary condition (PBC) and the open boundary condition (OBC). The specific results are shown in Fig. 9. For the case of $d = 0$, the system is Hermitian and satisfies the bulk-boundary correspondence, with the OBC and PBC energy spectra being consistent with each other [see Fig. 9(a)]. However, the system does not have disorder; most of the eigenstates of the Hermitian case are extended. As the disorder strength d increases, the PBC energy spectrum gradually deforms. However, as d further increases, the energy spectra under PBC and OBC once again coincide near the band-edge states. This progression signifies a competition between nonreciprocal coupling and disorder. For instance, in Fig. 9(b), when $d = 1.0$, the PBC and OBC energy spectra are no longer perfectly correlated. The eigenstates near the band edges of the energy spectra of the two conditions still coincide, and they are in the disorder-induced bulk localized phase, while the PBC energy spectra near the lower-energy states and near zero-energy states are gradually deformed, presenting a localized phenomenon similar to the non-Hermitian skin effect, which we define as the energy-dependent skin effect in Fig. 8. This indicates that disorder does not entirely affect the nonreciprocal coupling of the system. As the strength of disorder further increases, such as the case of $d = 1.5$ in Fig. 9(c), a greater number of states regain the coincidence of OBC and PBC energy spectra, and the range of the energy-dependent skin effect gradually decreases. This phenomenon is also observed

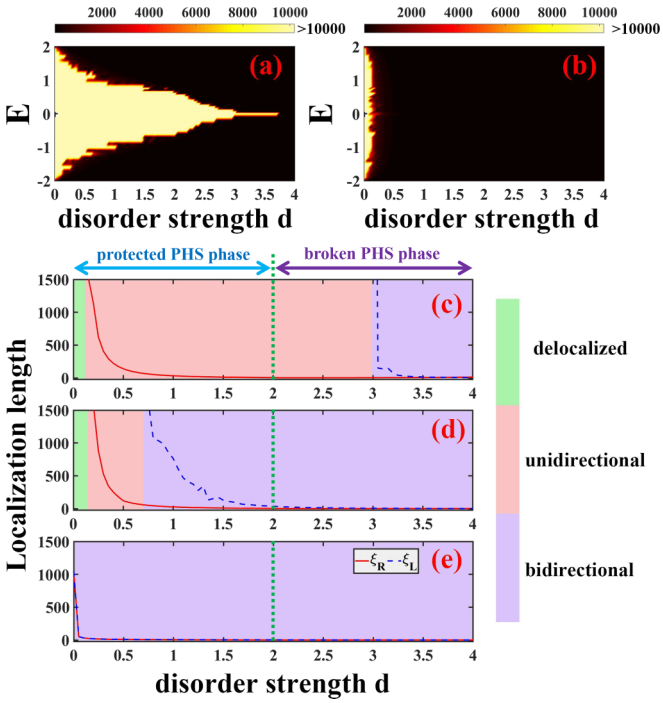

FIG. 10. (a),(b) The left and right localization lengths (ξ_L and ξ_R) diagram spectra of eigenenergy-disorder ($E - d$) respectively. (c)–(e) The left and right localization lengths for $L = 10\,000$ in the protected PHS phase and the broken PHS phase at energy $E = 0.05$, 1.0, and 2.0, respectively. The red solid line indicates ξ_R, and the blue dotted line corresponds to ξ_L. In (c)–(e), the green region means the delocalized states, the pink region represents the states that satisfy unidirectional localization, and the purple regions indicate the states that satisfy bidirectional localization.

in the broken PHS phase, but the region of the energy-dependent skin effect is smaller compared to the protected PHS phase. This implies that the disorder-induced localization effect gradually prevents the skin effect of nonreciprocal coupling. Therefore, we can conclude that the emergence of the energy-dependent skin effect of the system arises from a competitive action of disorder and nonreciprocal coupling, which is related to the deformation of the PBC energy spectrum.

Next, we focus on the long chain structure and calculate the localization lengths of the system at different energies in order to determine the localization characteristics of this system. In Figs. 10(a) and 10(b), we plot the diagrams of the left and right localization lengths ξ_L and ξ_R of eigenenergy-disorder ($E - d$), respectively. Unlike H_1, which shows a localization transition only in the protected PHS phase region, in the H_2 model, both the protected PHS phase and the broken PHS phase show a certain phenomenon of localization transition. Surely, this phenomenon is also different from the conclusion of 1D Anderson localization.

On the one hand, we discuss the phenomena in the protected PHS phase, and the specific results are shown in Figs. 10(c)–10(e). We can find that when disorder is weak, not all states are localized immediately, and the states close to the band edges undergo localization first, which is similar to H_1. When the disorder increases, the eigenstates of different energies exhibit approximately three different localization phenomena. The first is relevant to the near-zero-energy states, such as $E = 0.05$ in Fig. 10(c). We can see that $\xi_L \to \infty$ and $\xi_R \to \infty$ in the case of $0 < d < 0.13$, indicating the delocalized states in the system (green region). With the increase of d, the right localization length ξ_R remains finite and tends to zero following the enhancement of disorder. But at the same time, the left localization length ξ_L diverges with the increase of disorder strength. This suggests that the system undergoes unidirectional localization characteristics (pink region). This result is consistent with the energy-dependent NHSE in Fig. 8. Thus, the system undergoes a transition from delocalization to unidirectional localization. The second is for the lower-energy states, e.g., Fig. 10(d) with $E = 1.0$. It shows two types of localization processes in the system: following the increase of d, the system shows a transition from delocalization to unidirectional localization, which is similar to $E = 0.05$. As the disorder strength further increases, the localization length gradually satisfies $\xi_L < L$ and tends to zero. At this stage, ξ_L and ξ_R both exhibit localization effects, which we called bidirectional localization (purple region). Thus, the effect of unidirectional-to-bidirectional localization occurs, which is the second transition process. The third is for the higher-energy states, especially band-edge states. The disorder conditions for their localization in the left and right directions tend to be similar. For example, in Fig. 10(e), when $E = 2.0$, the system shows localization phenomena in the left and right directions. Regrading the broken PHS phase, the localization transition only appears in the region of the near-zero-energy states, and most of the states present bidirectional localization.

Based on the above results, we can summarize the conformational properties of H_2 in terms of localization and band structure: For the band structure, disorder leads to the existence of protected and broken PHS phases, and the pseudo-Hermitian phase transition is bounded by $d = 2t$.

For these two types of phases, they display different localization phenomena in the wave function: (I) In the protected PHS phase, the disorder drives the energy-dependent NHSE in the lower-energy region. With the increase of disorder, such a skin effect becomes more obvious, while it could transform into the whole-chain localization similar to that of the higher-energy states. (II) In the broken PHS phase, the energy-dependent NHSE can be observed, characterized by the double peaks near the absolute minimum of energy at which better localization occurs. Overall, when the left and right nonreciprocal disorders have different strengths, the skin effect occurs, but it is different from the traditional NHSE in which all states are localized on one side. The new NHSEs of the system are energy-dependent, with their main appearance at lower and near-zero energies.

Finally, as can be seen from the localization length, the two types of phases exhibit different localization transitions. The disorder likewise does not immediately render the localization. In addition, the unidirectional localization occurs in the region near zero energy, and the change from unidirectional to bidirectional localization is formed near the critical value. In the higher-energy band, the states still show the bidirectional localization feature. The appearance of the localization transition indicates that the localization is different from the traditional 1D Anderson localization.

TABLE I. Summary of band structures and localizations in the two configurations. In this table, "Condition" refers to the condition under which the system undergoes the PHS phase transition. "Disorder-averaged probability density" indicates the trend of disorder-averaged probability density in the short chain, and the left and right sides means the disorder-averaged probability density has a tendency to localize on the left and right sides of the system. These results correspond with Figs. 5 and 8. "Localization transition" indicates the process of localization transition in the long chain with the increase of disorder, and these results correspond with Figs. 6 and 10.

Case	Condition	Phase	Energy region	Disorder-averaged probability density	Localization (d increases)
H_1 [Ranges of W_1 and W_2 are same]	d=2t	PPHS [Im(E)=0]	higher-energy	middle	delocalized→bidirectional bidirectional (band edge state)
			lower-energy	weak left and right sides	delocalized→bidirectional
			near zero energy	left and right sides	
		BPHS [Im(E)≠0]	higher-energy	middle	bidirectional
			lower-energy	middle	
			near zero energy	weak left and right ends	
H_2 [Ranges of W_1 and W_2 are different]	d=2t	PPHS [Im(E)=0]	higher-energy	middle	delocalized→bidirectional bidirectional (band edge state)
			lower-energy	energy-dependent NHSE→middle	delocalized→unidirectional→bidirectional
			near zero energy	energy-dependent NHSE	delocalized→unidirectional
		BPHS [Im(E)≠0]	higher-energy	middle	bidirectional
			lower-energy	energy-dependent NHSE→middle	unidirectional→bidirectional
			near zero energy	energy-dependent NHSE→middle	unidirectional→bidirectional

IV. SUMMARY

To summarize, in this work we have investigated the localization phenomena in a 1D quantum chain that are driven by nonreciprocal disorder. We discuss in detail the impact of competing interactions between disorder and nonreciprocal coupling on the system's localization transition and skin effect. We found that such disorder plays a special role in driving the NHSE and state localization of this system. When the disorder strength is the same in the two hopping directions, the average probability densities of disorder in the low-energy and near-zero-energy states show a tendency to localize on both the left and right sides of the system in both the protected and broken PHS phases. More interestingly, the localization transition also appears in the case of weak disorder, with features related to the energy of the states. When the parameters of disorder in the two hopping directions are different, the energy-dependent NHSE is induced, which is a different localization phenomenon from the conventional NHSE. Moreover, the localization phenomenon becomes intricate with the emergence of a variety of localization transitions, such as delocalization-unidirectional-bidirectional localization. Table I presents the dominant phenomena in these structures in order to facilitate an understanding of the obtained results. The goal of our work is to present the interaction between nonreciprocity and disorder, and to enhance the understanding of the nonreciprocal disorder effect on 1D quantum systems.

In addition to the interesting results of our considered system, we would like to highlight its experimental achievement. In experiment, nonreciprocal coupling systems can now be realized using topological circuits [90–92]. By combining a capacitor and a negative impedance converter with current inversion or an operational amplifier, a nonreciprocal hopping term between the nearest sites is achieved [93,94]. The system's energy spectrum structure and local phenomena can be seen by examining the physical quantities of the circuits, such as the conductivity spectrum and the nonlocal voltage response. In addition, the desired disorder can be directly achieved by introducing some impurities at random and artificially during the fabrication of circuit boards [95]. Furthermore, the non-Hermitian topological Anderson insulator is simulated by using disordered photonic quantum walks, and its localization and topological properties are characterized [96]. The disordered non-Hermitian SSH model can be realized using photons in coupled microring cavities [97–99]. Therefore, our model can be realized in realistic experimental systems.

ACKNOWLEDGMENTS

This work was financially supported by the LiaoNing Revitalization Talents Program (Grant No. XLYC1907033), the National Natural Science Foundation of China (Grants No. 11905027 and No. 12104183), the Natural Science Foundation of Liaoning province (Grant No. 2023-MS-072), and

the Fundamental Research Funds for the Central Universities (Grant No. N2405001).

APPENDIX A: EXPLANATION ON THE CONDITION OF $d = 2t$ IN H_1 AND H_2

From the energy band spectra (Figs. 2, 3, and 7), we can conclude that the boundary between the protected and broken PHS phases is $d = 2t$. For this underlying reason, we would like to present our explanation from the standpoint of the left and right hopping terms.

For the configuration of H_1, according to Eq. (2), the system Hamiltonian can be expressed as a non-Hermitian tridiagonal matrix in an open boundary condition, and the upper and lower subdiagonal elements are not equal to zero. Based on previous works [80], all eigenvalues of H are real if all the products of the upper and lower diagonal elements are positive for the tridiagonal form matrix H, i.e., $b_n c_n > 0$. In the configuration of H_1, $b_n \equiv t + \frac{d}{2}W_{1,n}$ and $c_n \equiv t - \frac{d}{2}W_{2,n}$ with $W_{1,n}, W_{2,n} \in [-1.0, 1.0]$. Thus, we can obtain the expression $(t + d/2)(t - d/2) > 0$, with the solution being $-2t < d < 2t$. Since we set the disorder strength d to be larger than zero, the condition that satisfies this theorem for H_1 is $0 < d < 2t$. Therefore, the condition for the PHS phase transition is exactly defined as $d = 2t$ in H_1.

With a similar method, we can explain the PHS phase-transition condition in H_2. In such a case, $b_n \equiv t + \frac{d}{2}W_{1,n}$, $c_n \equiv t - \frac{d}{2}W_{2,n}$, and $W_{1,n} \in [-1.0, 1.0]$ and $W_{1,n} \in [-0.5, 0.5]$. We can obtain two relational equations, i.e., $(t + d/2)(t - d/4) > 0$ and $(t - d/2)(t + d/4) > 0$. The solutions are given as $-2t < d < 4t$ and $< -4t < d < 2t$, respectively. By defining the disorder strength to be greater than zero, we also obtain the condition $0 < d < 2t$, which is the same as H_1. Thus, for the configuration of H_2, the condition of the PHS phase transition is also described as $d = 2t$.

APPENDIX B: LEVEL STATISTICS s

From Fig. 6, we know that the system H_1 can display localization effects. According to the random matrix theory, delocalization and localization states can be characterized by energy level statistics [100,101]. In the non-Hermitian case, we can calculate the level statistics of real eigenvalues [66] to verify the localization of the system under different disorder strengths. The calculated expression for energy level statistics

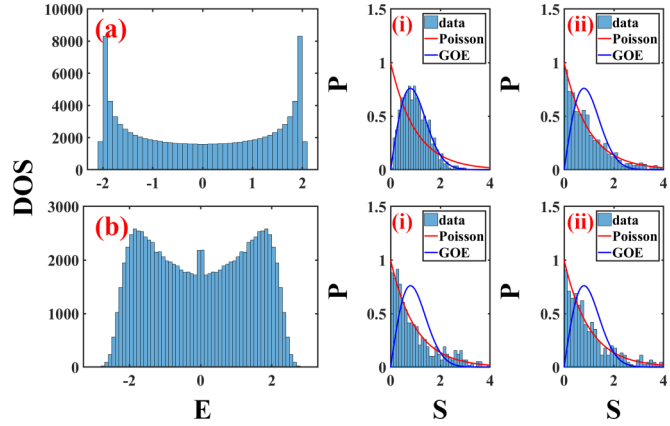

FIG. 11. (a),(b) Spectra of the density of states for $d = 0.1$ and 1.5. (i),(ii) Energy level statistics of real eigenvalues for $E = 0.2$ and 2.0.

can be given as

$$s = \frac{S}{\langle S \rangle} = \frac{E_{n+1} - E_n}{\langle E_{n+1} - E_n \rangle}. \tag{B1}$$

The average value $\langle \cdots \rangle$ in the denominator represents the overall average value, and E_n are real eigenvalues. In Fig. 11, we verify the localization effects of our system by studying the energy level statistics. The density of states and level histograms are plotted in Figs. 11(a) and 11(b) with $d = 0.1$ and 1.5. When $d = 0.1$ [shown in Fig. 11(a)], it can be found from the density of states that all the eigenvalues are mainly concentrated within the limit of $|E| = 2.0$, while their densities are lower at the center. In the case of $d = 1.5$, as shown in Fig. 11(b), the eigenvalues are localized near $E = 0$ in addition to the localization in the high-energy regions. To be specific, in Fig. 11(a)(i), the histograms are close to the Gaussian orthogonal ensemble, i.e., $p(s) = (\pi/2)s \exp[-(\pi/4)s^2]$. This means that the eigenstates are delocalized states. With an increase of d, such as $d = 1.5$ [see Fig. 11(b)(i)], the eigenstates are trended to show a Poisson distribution, i.e., $p(s) = \exp(-s)$, implying that the states are localized. Therefore, we find that the system undergoes a localization transition with an increase of d. For states close to the band edges, e.g., $E = 2.0$ in Figs. 11(a)(iii) and 11(b)(iii), whether $d = 0.1$ or 1.5, the energy level statistics satisfies the Poisson distribution. It is shown that the band-edge states are more likely to be localized compared to lower energy states. These results can be consistent with the results of the localization length.

[1] P. W. Anderson, Phys. Rev. **109**, 1492 (1958).
[2] E. Abrahams, P. W. Anderson, D. C. Licciardello, and T. V. Ramakrishnan, Phys. Rev. Lett. **42**, 673 (1979).
[3] P. A. Lee and T. V. Ramakrishnan, Rev. Mod. Phys. **57**, 287 (1985).
[4] J. Billy, V. Josse, Z. Zuo, A. Bernard, B. Hambrecht, P. Lugan, D. Cèment, L. Sanchez-Palencia, P. Bouyer, and A. Aspect, Nature (London) **453**, 891 (2008).
[5] M. Segev, Y. Silberberg, and D. N. Christodoulides, Nat. Photon. **7**, 197 (2013).
[6] G. Roati, C. D'Errico, L. Fallani, M. Fattori, C. Fort, M. Zaccanti, G. Modugno, M. Modugno, and M. Inguscio, Nature (London) **453**, 895 (2008).
[7] F. Evers and A. D. Mirlin, Rev. Mod. Phys. **80**, 1355 (2008).
[8] Y. Liu, Q. Zhou, and S. Chen, Phys. Rev. B **104**, 024201 (2021).
[9] S. Aubry and G. André, Ann. Isr. Phys. Soc. **3**, 133 (1980).
[10] J. Biddle, B. Wang, D. J. Priour, Jr., and S. Das Sarma, Phys. Rev. A **80**, 021603(R) (2009).

[11] H. P. Lüschen, S. Scherg, T. Kohlert, M. Schreiber, P. Bordia, X. Li, S. DasSarma, and I. Bloch, Phys. Rev. Lett. **120**, 160404 (2018).

[12] H. M. Guo, G. Rosenberg, G. Refael, and M. Franz, Phys. Rev. Lett. **105**, 216601 (2010).

[13] J. H. Zheng, T. Qin, and W. Hofstetter, Phys. Rev. B **99**, 125138 (2019).

[14] R. Chen, D. H. Xu, and B. Zhou, Phys. Rev. B **100**, 115311 (2019).

[15] J. Li, R.-L. Chu, J. K. Jain, and S. Q. Shen, Phys. Rev. Lett. **102**, 136806 (2009).

[16] R. Wakatsuki, M. Ezawa, Y. Tanaka, and N. Nagaosa, Phys. Rev. B **90**, 014505 (2014).

[17] E. Prodan and H. Schulz-Baldes, *Mathematical Physics Studies* (Springer, New York, 2016).

[18] V. M. Martinez Alvarez and M. D. Coutinho-Filho, Phys. Rev. A **99**, 013833 (2019).

[19] J. K. Asbóth, L. Oroszlány, and A. Pályi, *Lecture Notes in Physics* (Springer, New York, 2016).

[20] C.-K. Chiu, J. C. Y. Teo, A. P. Schnyder, and S. Ryu, Rev. Mod. Phys. **88**, 035005 (2016).

[21] H. Jiang, L. Wang, Q.-F. Sun, and X. C. Xie, Phys. Rev. B **80**, 165316 (2009).

[22] J. Song and E. Prodan, Phys. Rev. B **89**, 224203 (2014).

[23] X. Shi, I. Kiorpelidis, R. Chaunsali, V. Achilleos, G. Theocharis, and J. Yang, Phys. Rev. Res. **3**, 033012 (2021).

[24] C.-B. Hua, R. Chen, D.-H. Xu, and B. Zhou, Phys. Rev. B **100**, 205302 (2019).

[25] J. He, J.-R. Li, L. L. Zhang, S.-F. Zhang, and W.-J. Gong, Eur. Phys. J. Plus **137**, 935 (2022).

[26] C. M. Bender, D. C. Brody, and H. F. Jones, Phys. Rev. Lett. **89**, 270401 (2002).

[27] V. V. Konotop, J. Yang, and D. A. Zezyulin, Rev. Mod. Phys. **88**, 035002 (2016).

[28] Y. Ashida, Z. Gong, and M. Ueda, Adv. Phys. **69**, 249 (2020).

[29] S. K. Özdemir, S. Rotter, F. Nori, and L. Yang, Nat. Mater. **18**, 783 (2019).

[30] C. Wu, N. Liu, G. Chen, and S. Jia, Phys. Rev. A **106**, 012211 (2022).

[31] W.-J. Geng, Y.-J. Wang, Z.-X. Zhang, J. Cao, W.-X. Cui, and H.-F. Wang, Phys. Rev. B **108**, 144109 (2023).

[32] L. Jin, P. Wang, and Z. Song, Sci. Rep. **7**, 5903 (2017).

[33] S. Garmon and K. Noba, Phys. Rev. A **104**, 062215 (2021).

[34] A. F. Tzortzakakis, A. Katsaris, N. E. Palaiodimopoulos, P. A. Kalozoumis, G. Theocharis, F. K. Diakonos, and D. Petrosyan, Phys. Rev. A **106**, 023513 (2022).

[35] A. Yoshida, Y. Otaki, R. Otaki, and T. Fukui, Phys. Rev. B **100**, 125125 (2019).

[36] Y. Zhang and S. Chen, Phys. Rev. B **107**, 224306 (2023).

[37] C. M. Bender and S. Boettcher, Phys. Rev. Lett. **80**, 5243 (1998).

[38] C. M. Bender, Rep. Prog. Phys. **70**, 947 (2007).

[39] Y. Xing, L. Qi, J. Cao, D. Y. Wang, C. H. Bai, H. F. Wang, A. D. Zhu, and S. Zhang, Phys. Rev. A **96**, 043810 (2017).

[40] J.-R. Li, Z.-A. Wang, T.-T. Xu, L.-L. Zhang, and W.-J. Gong, Prog. Theor. Exp. Phys. **2023**, 023I01 (2023).

[41] L. Jin, Phys. Rev. A **96**, 032103 (2017).

[42] K. Kawabata, Y. Ashida, H. Katsura, and M. Ueda, Phys. Rev. B **98**, 085116 (2018).

[43] X. S. Li, Z. Z. Li, L. L. Zhang, and W. J. Gong, J. Phys.: Condens. Matter **32**, 165401 (2020).

[44] L. L. Zhang, J. R. Li, D. Zhang, T. T. Xu, W. B. Cui, and W. J. Gong, Results Phys. **34**, 105274 (2022).

[45] X. M. Zhao, C. X. Guo, S. P. Kou, L. Zhuang, and W. M. Liu, Phys. Rev. B **104**, 205131 (2021).

[46] C. Yuce and H. Ramezani, Phys. Rev. A **100**, 032102 (2019).

[47] J.-R. Li, L.-L. Zhang, W.-B. Cui, and W.-J. Gong, Phys. Rev. Res. **4**, 023009 (2022).

[48] A. Stegmaier, S. Imhof, T. Helbig, T. Hofmann, C. H. Lee, M. Kremer, A. Fritzsche *et al.*, Phys. Rev. Lett. **126**, 215302 (2021).

[49] Z. Lin, J. Schindler, F. M. Ellis, and T. Kottos, Phys. Rev. A **85**, 050101(R) (2012).

[50] L. Su, H. Jiang, Z. Wang, S. Chen, and D. Zheng, Phys. Rev. B **107**, 184108 (2023).

[51] L. Lu, J. D. Joannopoulos, and M. Soljačić, Nat. Photon. **8**, 821 (2014).

[52] M. G. Silveirinha, Phys. Rev. B **99**, 125155 (2019).

[53] T. Ozawa, H. M. Price, A. Amo, N. Goldman, M. Hafezi, L. Lu, M. C. Rechtsman, D. Schuster, J. Simon, O. Zilberberg, and I. Carusotto, Rev. Mod. Phys. **91**, 015006 (2019).

[54] L. Feng, R. El-Ganainy, and L. Ge, Nat. Photon. **11**, 752 (2017).

[55] A. Regensburger, C. Bersch, M. A. Miri, G. Onishchukov, D. N. Christodoulides, and U. Peschel, Nature (London) **488**, 167 (2012).

[56] Y. Wu, B. Zhu, S. F. Hu *et al.*, Front. Phys. **12**, 121102 (2017).

[57] S. Yao and Z. Wang, Phys. Rev. Lett. **121**, 086803 (2018).

[58] S. Yao, F. Song, and Z. Wang, Phys. Rev. Lett. **121**, 136802 (2018).

[59] X. Zhu, H. Wang, S. K. Gupta, H. Zhang, B. Xie, M. Lu, and Y. Chen, Phys. Rev. Res. **2**, 013280 (2020).

[60] J.-R. Li, C. Jiang, H. Su, D. Qi, L.-L. Zhang, and W.-J. Gong, Front. Phys. **19**, 33204 (2024).

[61] R. Lin, T. Tai, L. Li, and C. H. Lee, Front. Phys. **18**, 53605 (2023).

[62] Y. Xiong, J. Phys. Commun. **2**, 035043 (2018).

[63] T. S. Deng and W. Yi, Phys. Rev. B **100**, 035102 (2019).

[64] F. Song, S. Yao, and Z. Wang, Phys. Rev. Lett. **123**, 246801 (2019).

[65] K. Yokomizo and S. Murakami, Phys. Rev. Lett. **123**, 066404 (2019).

[66] Z. Xiao, K. Kawabata, X. Luo, T. Ohtsuki, and R. Shindou, Phys. Rev. Res. **4**, 043196 (2022).

[67] C. Zhang, L. Sheng, and D. Y. Xing, Phys. Rev. B **103**, 224207 (2021).

[68] A. Moustaj, L. Eek, and C. Morais Smith, Phys. Rev. B **105**, L180503 (2022).

[69] N. Hatano and D. R. Nelson, Phys. Rev. Lett. **77**, 570 (1996).

[70] K. Kawabata and S. Ryu, Phys. Rev. Lett. **126**, 166801 (2021).

[71] N. Hatano and D. R. Nelson, Phys. Rev. B **58**, 8384 (1998).

[72] P. W. Brouwer, P. G. Silvestrov, and C. W. J. Beenakker, Phys. Rev. B **56**, R4333 (1997).

[73] A. A. Zyuzin and A. Yu. Zyuzin, Phys. Rev. B **97**, 041203(R) (2018).

[74] S. Longhi, Phys. Rev. B **103**, 144202 (2021).

[75] H. Jiang, L.-J. Lang, C. Yang, S.-L. Zhu, and S. Chen, Phys. Rev. B **100**, 054301 (2019).

[76] K. M. Kim and M. J. Park, Phys. Rev. B **104**, L121101 (2021).

[77] P. Molignini, O. Arandes, and E. J. Bergholtz, Phys. Rev. Res. **5**, 033058 (2023).
[78] S. Longhi, Opt. Lett. **45**, 5250 (2020).
[79] G. Marinello and M. P. Pato, J. Phys.: Conf. Ser. **738**, 012040 (2016).
[80] O. Bohigas and M. P. Pato, AIP Adv. **3**, 032130 (2013).
[81] Q.-B. Zeng and R. Lü, Phys. Rev. B **105**, 245407 (2022).
[82] F. Wegner, Z. Phys. B **36**, 209 (1980).
[83] L. W. Zhou, Phys. Rev. B **108**, 014202 (2023).
[84] J.-R. Li, L.-L. Zhang, C.-H. Zhao, S.-F. Zhang, Y.-L. Zhu, and W.-J. Gong, Phys. Rev. B **109**, 165407 (2024).
[85] M. L. Mehta, *Random Matrices*, 2nd ed. (Academic, Boston, 1991).
[86] W.-J. Zhang, Y.-P. Wu, L.-Z. Tang, and G.-Q. Zhang, Commun. Theor. Phys. **74**, 075702 (2022).
[87] D. W. Zhang, L. Z. Tang, L. J. Lang *et al.*, Sci. China Phys. Mech. Astron. **63**, 267062 (2020).
[88] D. J. Thouless, Phys. Rep. **13**, 93 (1974).
[89] P. W. Anderson, D. J. Thouless, E. Abrahams, and D. S. Fisher, Phys. Rev. B **22**, 3519 (1980).
[90] H. Yuan, W. Zhang, Z. Zhou, W. Wang, N. Pan, Y. Feng, H. Sun, and X. Zhang, Adv. Sci. **10**, 2301128 (2023).
[91] T. Helbig, T. Hofmann, S. Imhof *et al.*, Nat. Phys. **16**, 747 (2020).
[92] D. Zou, T. Chen, W. He *et al.*, Nat. Commun. **12**, 7201 (2021).
[93] W. K. Chen, *The Circuits and Filters Handbook*, 3rd ed. (CRC, Boca Raton, FL, 2019).
[94] K. Xu, X. Zhang, K. Luo, R. Yu, D. Li, and H. Zhang, Phys. Rev. B **103**, 125411 (2021).
[95] X.-X. Bao, G.-F. Guo, X.-P. Du, H.-Q. Gu, and L. Tan, J. Phys.: Condens. Matter **33**, 185401 (2021).
[96] Q. Lin, T. Li, L. Xiao, K. Wang, W. Yi, and P. Xue, Nat. Commun. **13**, 3229 (2022).
[97] M. A. Bandres, S. Wittek, G. Harari, M. Parto, J. Ren, M. Segev, D. N. Christodoulides, and M. Khajavikhan, Science **359**, eaar4005 (2018).
[98] S. Longhi, D. Gatti, and G. D. Valle, Sci. Rep. **5**, 13376 (2015).
[99] X.-W. Luo and C. Zhang, Appl. Phys. Lett. **123**, 081111 (2023).
[100] M. L. Mehta, *Random Matrices*, 2nd ed. (Academic Press, Boston, 1991).
[101] C.-Z. Chen, H. Liu, H. Jiang, Q.-F. Sun, Z. Wang, and X. C. Xie, Phys. Rev. B **91**, 214202 (2015).